Optical Materials 62 (2016) 95–103

Contents lists available at ScienceDirect

Optical Materials

journal homepage: www.elsevier.com/locate/optmat

Thermal, structural and optical properties of new TeO_2–Sb_2O_3–GeO_2 ternary glasses

C. Pereira [a], J. Barbosa [a], F.C. Cassanjes [a], R.R. Gonçalves [b], S.J.L. Ribeiro [c], G. Poirier [a, *]

[a] Grupo de Química de Materiais, Universidade Federal de Alfenas, Campus de Poços de Caldas, Poços de Caldas, MG, Brazil
[b] Departamento de Química, Faculdade de Filosofia, Ciências e Letras de Ribeirão Preto, Universidade de São Paulo, Av. Bandeirantes, 3900, 14040-901, Ribeirão Preto, SP, Brazil
[c] Instituto de Química, Universidade Estdual Paulista Júlio de Mesquita Filho, Araraquara, SP, Brazil

ARTICLE INFO

Article history:
Received 16 May 2016
Received in revised form
9 September 2016
Accepted 19 September 2016
Available online 28 September 2016

Keywords:
Glass
Tellurite
Germanate
Antimony
Luminescence

ABSTRACT

In this work the novel glass system TeO_2–Sb_2O_3–GeO_2 was investigated and promising glass compositions were selected for further specific studies. Glass samples in the (80-0.8x)TeO_2-(20-0.2x)Sb_2O_3 –xGeO_2 molar composition were prepared by the melt-quenching method with a glass-forming domain from x = 10 to x = 90. Samples were investigated by XRD, DSC, FTIR, Raman spectroscopy and UV–visible absorption. The XRD and DSC results bring informations about the non-crystalline state and thermal properties of these materials. It has been observed that higher GeO_2 contents lead to higher glass transition temperatures and thermal stabilities against crystallization. FTIR and Raman spectroscopies suggest a progressive incorporation of GeO_2 in the covalent network of TeO_2 with conversion of structural units TeO_4 to TeO_3. Absorption spectra revealed the high visible transparency of these samples and an increase of the optical band gap with GeO_2 addition, in agreement with a decreasing polarizability of the glass network. Er^{3+} doped and Er^{3+}/Yb^{3+} codoped samples were also studied with respect to their infrared emission properties and higher GeO_2 contents lead to an increase in IR emission intensity at 1,5 μm as well as longer radiative lifetimes. Finally, upconversion emission in the visible were also recorded and were shown to be strongly dependent of the composition.

1. Introduction

TeO_2 based glasses are the subject of many studies since the first reports of tellurite glasses by Stanworth and co-workers [1,2]. These materials have many characteristics that generate scientific and technological interest such as non-linear refractive index, high dielectric constant, low phonon energies among oxide glasses and low melting points (around 800 °C, depending of composition) [3,4]. The refractive index of these glasses make these materials candidates for fabrication of nonlinear optical devices due to lone electrons pair responsible for polarizability changes [5–9]. On the other hand, low phonon energy value causes higher transmission in the infrared region and higher luminescence efficiency of rare earth ions [10,11]. These properties make tellurite glasses excellent candidates for fabrication of fiber optic amplifiers and glass-ceramics for optics.

The addition of glass former GeO_2 can cause changes in physicochemical and optical properties of tellurite glasses. For example, increasing GeO_2 contents usually produce higher thermal stability and these compositional modifications can change the covalence environment that influences photoluminescence and optical properties [12–19]. GeO_2 addition can also induce photo-structural effects, such as refractive index changes due to photo-induced phenomena. Hence germanate glasses are used to generate phase gratings directly in optical fibers by UV irradiation [20]. In addition, these materials are also promising candidates for solid electrolyte applications [21] because of their high ionic conductivities. Many studies of structural changes in GeO_2 based glasses are available in the literature. These studies point out that GeO_2 participates in the glass network through GeO_4 and GeO_6 structural units [22–26].

Sb_2O_3 incorporation further opens the range of applications. It is seen that antimoniate glasses exhibits high polarizability that enhances the refractive index values. Hence, TeO_2 based glasses containing Sb_2O_3 have a large number of applications that include

* Corresponding author. Instituto de Ciência e Tecnologia, Campus de Poços de Caldas – UNIFAL-MG, Rodovia José Aurélio Vilela 11999, Cidade Universitária, CEP 37715-400 Poços de Caldas, MG, Brazil.
E-mail address: gael.poirier@unifal-mg.edu.br (G. Poirier).

http://dx.doi.org/10.1016/j.optmat.2016.09.055
0925-3467/

three-dimensional photonic devices for integrated optics and specific nonlinear optical devices such as ultrafast optical switches and power limiters [27,28]. These glasses can also find applications in broad band optical amplifiers operating around 1.5 μm as antimony-silicate glass fibers and also for amplification of other telecommunication bands (1530–1560 nm) [29,30].

The understanding of chemical, structural and thermal properties of a glass composition is a key point for application in optics and studies of new glass systems can lead to the development of innovative materials. In this paper we investigated thermal, structural and photoluminescent properties of new ternary glasses in the system TeO_2–Sb_2O_3–GeO_2. We focused on evaluating the possibility of obtaining rare-earth undoped and doped glass samples containing increasing GeO_2 contents. The promising and stable compositions (80-0.8x) TeO_2 - (20-0.2x) Sb_2O_3 - xGeO_2 were investigated. Three sets of samples were prepared: 1-undoped glasses with x from 10 to 90 for thermal and structural studies; 2- Er_2O_3 doped glasses and 3- Er_2O_3/Yb_2O_3 codoped glasses for photoluminescence studies.

2. Experimental part

2.1. Glass synthesis

The ternary glasses were prepared by traditional melt-quenching in the ternary system (80-0.8x)TeO_2-(20-0.2x)Sb_2O_3-xGeO_2 with *x* varying from 10 to 90. Some samples were doped with 0,1%Er_2O_3 and codoped with 0,1%Er_2O_3/0,5%Yb_2O_3. In a first step, the precursor powders such as TeO_2 (99+ %, Aldrich), GeO_2 (99+ %, Aldrich), Sb_2O_3 (99+ %, Aldrich), Er_2O_3 and Yb_2O_3 were mixed, grinded in an agate mortar and melted in a covered Pt crucible to minimize losses due to sublimation at temperatures ranging from 850 °C to 1150 °C depending of composition. The melt was cooled in a steel mold preheated below the glass transition temperature and stable glasses samples were obtained. Three sets of samples were prepared: (1) undoped glasses, (2) 0,1% Er_2O_3-doped glasses and (3) 0,1%Er_2O_3/0,5%Yb_2O_3 codoped glasses. Some compositions resulted in dark samples, which is probably connected with redox processes between Sb and Te atoms and metallic tellurium precipitation. For these compositions, sodium nitrate $NaNO_3$ was added since the couple Sb_2O_3/$NaNO_3$ is known to promote oxygen release and oxidation of the melt. Colorless samples were obtained using this methodology.

2.2. Glass characterization

Glass samples were analyzed by X-ray diffraction with a Rigaku Ultima IV diffractometer using Cu Kα radiation. The 2θ investigation region was in the range of 3–70° with a step pass of 0,02° and a step time of 1s. Thermal analysis were performed using a DSC/TG calorimeter STA 449 F3 Jupiter from Netzsch, 50 mg of bulk samples were heated in Pt/Rh covered crucibles (10 K/min and 50 mL.min^{-1} of N_2 flux) in the range of 200–900 °C. Infrared absorption measurements were realized in powder samples using a spectrophotometer Thermo Scientific - IS-Nicolet FT-IR 50 in the 1300–400 cm^{-1} spectral range. Raman scattering measurements were recorded between 100 and 1200 cm^{-1} on bulk samples using a Jobin-Yvon Horiba-HR800 instrument, operating with a He/Ne-laser at 632,8 nm. Absorption spectra were recorded in the 200–2200 nm range using Agilent Cary 7000 spectrophotometer. Refraction index were obtained with Metricon M-line apparatus working at 534 nm Er^{3+} emission spectra in the infrared were obtained with a Horiba Jobin Yvon Fluorolog spectrofluorometer between 1400 nm and 1700 nm using a 450W Xe continuous lamp for excitation. The experimental conditions were slit excitation of 3 nm, slit emission of 2 nm with a step of 0,5 nm and acquisition time of 0,2s. For upconversion emission of Er^{3+} in the visible, a continuous solid state laser operating at 980 nm was used for excitation. Emission spectra were recorded between 500 nm and 700 nm using the same experimental conditions described below. For lifetimes measurement was used Xe pulsed lamp with 8 nm for excitation and emission slits and 0,05 nm delay increment.

3. Results

Glass samples were obtained by melt-quenching in the ternary system (80-0.8x)TeO_2-(20-0.2x)Sb_2O_3-xGeO_2 with x varying from 10 to 90. X-ray diffraction measurements presented in Fig. 1 are free of diffraction peaks and exhibited only the diffraction halo centered around $2\theta = 27{,}6°$ for sample 10Ge and a shift to lower angles for higher GeO_2 contents together with the appearance of a second diffraction halo around $2\theta = 37°$. DSC curves for undoped bulk glass samples are presented in Fig. 2 and molar compositions, glass transition temperatures, band gap energies, refractive indices and visual aspect of samples are listed in Table 1. Glass transition is clearly identified for all samples as an inflexion of the baseline related with heat capacity changes between the glass and viscoelastic states. These DSC measurements did not detect other thermal events between 250 °C and 800 °C but were not performed at higher temperatures because of a progressive mass loss detected above 800 °C by thermogravimetry.

Infrared spectra of the glass compositions presented in Fig. 3 allowed to identify a broad band centered around 620 cm^{-1} for samples 10Ge to 50Ge, attributed to stretchings of TeO_4 species [31–33]. When GeO_2 content is increased up to 50 mole%, another broad band around 850 cm^{-1} appears together with weak absorption bands at 760 cm^{-1} and 890 cm^{-1}. These signals are attributed to asymmetric stretching of bridging Ge–O–Ge bonds, symmetric and asymmetric stretchings of Ge–O$^-$ terminal bonds in GeO_4 tetrahedra respectively [34,35].

Raman measurements were also performed on the glass samples versus GeO_2 content as shown in Fig. 4. Sample 10Ge is

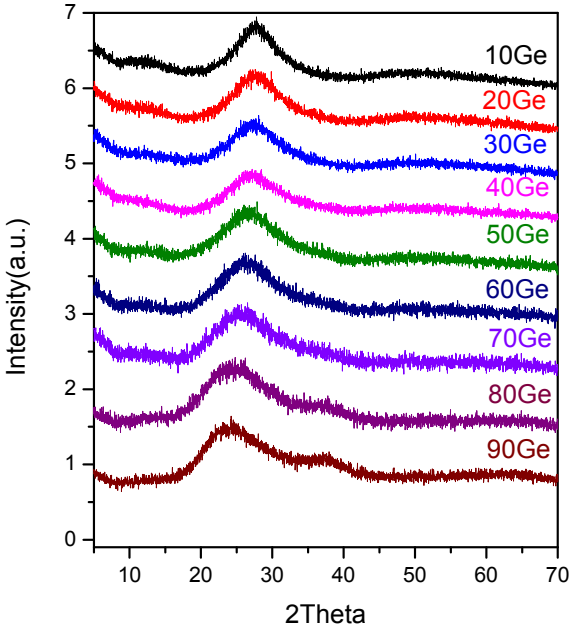

Fig. 1. X-ray diffraction patterns of samples in the ternary system 80%TeO_2–20%Sb_2O_3 (fixed proportion)-xGeO_2.

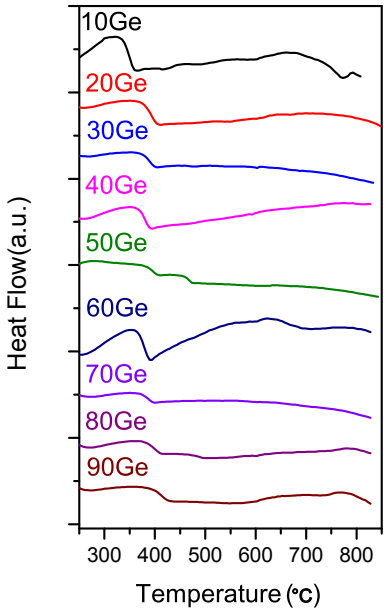

Fig. 2. DSC curves of samples in powder form.

dominated by three broad bands centered at 454, 670 and 748 cm^{-1} respectively. These signals are attributed to symmetric stretching vibration of Ge–O–Ge in six-membered rings made of six GeO_4 tetrahedra and stretchings of Te–O bonds in TeO_4 and TeO_3 units, respectively [36]. The signals attributed to tellurium oxide units progressively vanish with increasing GeO_2 contents whereas the Raman band due to Ge–O–Ge bridging bonds shifts to lower wavenumbers. Raman spectrum of sample 90Ge is mainly dominated by this latter signal [36].

Absorption spectra presented in Fig. 5 clearly point out that GeO_2 addition results in a higher transparency for glass samples with a shift of the optical cut-off of about 60 nm. For bandgap energies determination, these absorption spectra were used to calculate the absorption coefficient using the Beer-Lambert relation: $A = \alpha.c.l$, where A is the absorbance, α the absorption coefficient, c the concentration and l the optical path (thickness). The relation between α and incident photon energy ($h\nu$) for allowed indirect transitions is given by $\alpha h\nu = A(h\nu - E)^2$ where A is a constant and E is the indirect band gap [37]. Fig. 6 illustrates this data treatment with α as a function of incident photon energy in the near band gap region where the band gap value is obtained by the crossing point in x axis. Refractive indices were determined by the prism coupling M-Line technique. Both values are resumed in Table 1, showing that higher GeO_2 contents promote higher

Table 1
Compositions, glass transition temperature (Tg), refractive index under 543 nm, band gap and pictures of glass samples.

Samples	Picture	Molar concentration (100-x)[0,8TeO_2–20Sb_2O_3]-xGeO_2	Band gap/eV	Refractive index	Tg/°C
10Ge		10	–	–	328
20Ge		20	3,12	2,0041	378
30Ge	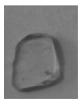	30	3,18	1,9891	381
40Ge		40	3,24	1,9523	364
50Ge		50	3,33	1,9004	388
60Ge		60	3,37	1,8511	364
70Ge		70	3,44	1,8010	370
80Ge		80	3,51	1,7344	383
90Ge		90	3,63	1,6942	390

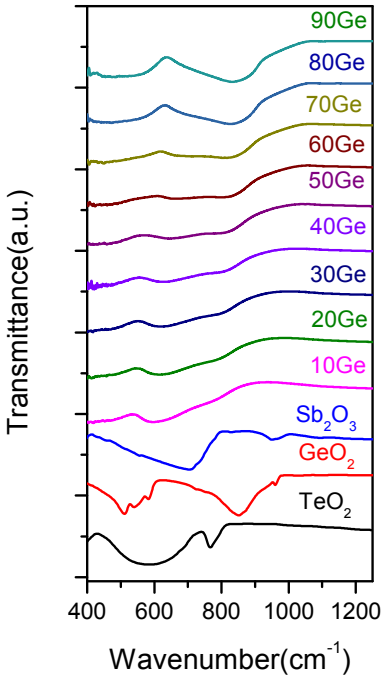

Fig. 3. FTIR spectra of glass samples and crystalline references GeO_2, Sb_2O_3 and TeO_2.

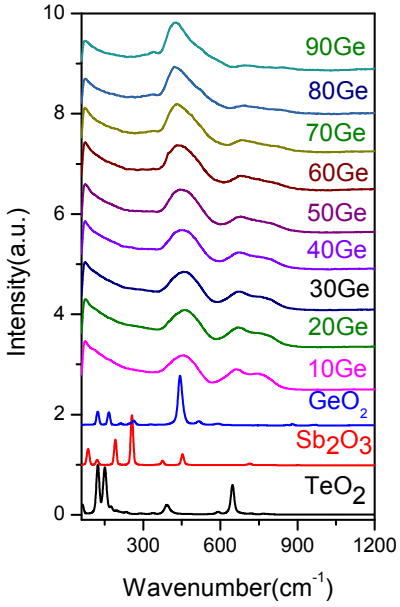

Fig. 4. Raman spectra of glass samples and crystalline reference GeO_2, Sb_2O_3 and TeO_2.

bandgap energies and lower refractive indices.

Emission spectra in the infrared by 980 nm excitation were also obtained for Er^{3+} doped and Er^{3+}/Yb^{3+} codoped samples as presented in Fig. 7. Since these measurements were performed on powder glass samples with controlled grain size using the same sample quantity for all samples, Fig. 7 allowed to determine higher emission intensities for Er^{3+}/Yb^{3+} codoped samples when compared to monodoped Er^{3+} samples as well as for higher GeO_2 contents. Results of upconversion emission in the visible for codoped samples under 980 nm laser excitation are resumed in Fig. 8 in which three main emission bands are observed around 524 nm, 546 nm and 657 nm. For a better comparison of the relative emission intensities versus glass composition, all upconversion spectra were normalized at the 546 nm emission band. This procedure allowed to identify an increase of the relative emission intensity at 657 nm when compared to the two other emissions at 524 nm and 546 nm. These two latter emissions do not exhibit any intensity ratio dependence versus glass composition. Finally, the dependence of excitation intensity on emission intensity has also been investigated for these upconversion emissions since it is well known that a graphic representation Log I (I being the emission intensity) in function of Log P (P being the excitation power) presents a linear dependence in which the slope gives the number of excitation photons n absorbed for each emission photon. For the three emission bands detected in the codoped glass samples, the slopes give n values around 2 (Fig. 9).

4. Discussion

Glass samples were prepared in the ternary system (80-0.8x) TeO_2-(20-0.2x) Sb_2O_3-xGeO_2 with *x* varying from 10 to 90 as shown in Table 1.

During synthesis, it has been observed that glass samples with low GeO_2 contents (10Ge and 20Ge) exhibited a dark color and low transparency whereas higher GeO_2 concentrations result in transparent colorless samples. Transparency losses in antimony tellurite glasses have already been reported and were attributed to redox processes related with Te^{4+} reduction to metallic tellurium and Sb^{3+} oxidation to Sb^{5+} [38]. For these glasses, small amounts of $NaNO_3$ were added to promote oxidizing conditions during melting. In fact, the couple $NaNO_3/Sb_2O_3$ is widely used in silicate glass manufacturing for refining and oxidation of reduced species. At lower temperature, antimony is oxidized by the nitrate:

$$4Sb_2O_3 + NaNO_3 \rightarrow 2\ Na_2O + Sb_2O_5 + 4\ NO_2$$

During melting at higher temperatures, Sb_2O_5 decomposes to Sb_2O_3 and releases O_2 which refines and oxidizes the glass melt. In our case, the starting powders were first treated at 400 °C for 1 h before melting and casting. This procedure allowed to increase the glass transparency of sample 10Ge and 20Ge as shown in Table 1.

Since the vitreous state of the prepared samples was only suspected based on visual observations, X-ray diffraction measurements were performed on undoped samples to check the presence or lack of crystalline phases precipitated during the sample synthesis. Diffraction patterns presented in Fig. 1 exhibit only diffraction halos characteristic of non-crystalline materials whereas diffraction peaks were not observed. The diffraction halo obtained for non-crystalline materials can be explained by X-ray scattering of the shortest bonds at the atomic scale. In fact, non-crystalline materials do not exhibit long range order but are ordered regarding to the first and second coordination shell. For this reason, the diffraction halo is related with the radial distribution function and each diffraction halo can be attributed to the shortest chemical bonds building the material. X-ray diffraction patterns shown in Fig. 1 are clearly dependent of the composition with a shift of the main diffraction halo to lower angles and appearance of a second diffraction halo around $2\theta = 37.2°$ for higher GeO_2 contents. This evolution is in agreement with a progressive change in the shortest chemical bonds with increasing GeO_2 contents. For example, the shortest chemical bonds responsible for X-ray scattering in sample 10Ge could be the Te–O and Sb–O bonds whereas sample 90Ge is mainly constituted of shorter Ge–O bonds.

DSC curves for undoped bulk glass samples are presented in Fig. 2 and molar compositions, glass transition temperature, refractive indices, band gap and visual aspect of samples are listed in Table 1. The only thermal event observed from these curves is the

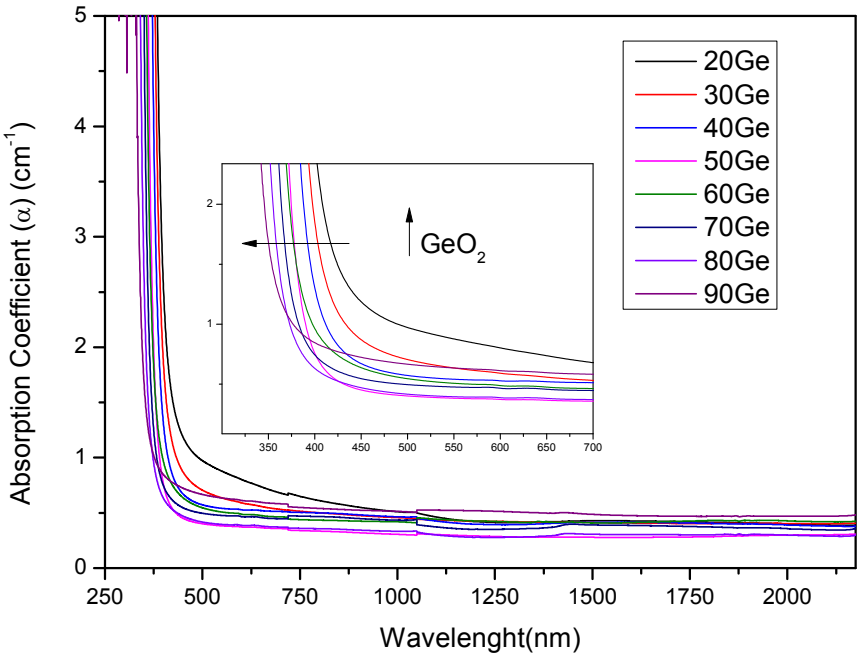

Fig. 5. UV–Vis–NIR absorption spectra of glass samples.

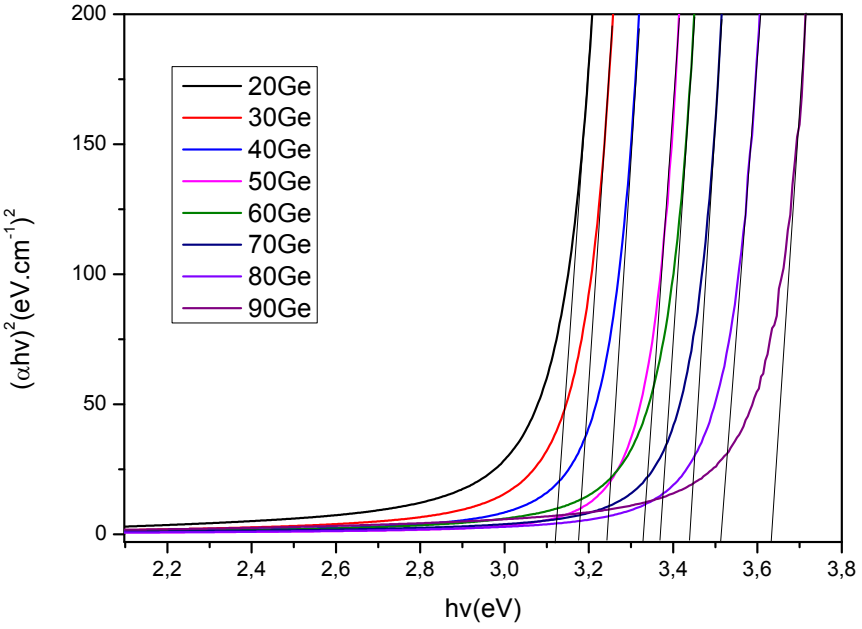

Fig. 6. $(\alpha h\nu)^2$ in function of incident photon energy for bandgap energy determinations.

glass transition identified as a baseline change. Exothermic events related with crystallization were not identified in the studied temperature range. For instance, this behavior suggests that GeO_2 addition lead to a higher thermal stability of these glass samples. The glass transition temperatures varied slightly with increases in GeO_2 concentration. This variation in Tg is related with two important parameters in glass structure which are the glass network connectivity and chemical bond strength. Higher Tg values indicate higher connectivity and/or stronger chemical bonds. According to glass compositions, GeO_2 is progressively incorporated in a $80TeO_2–20Sb_2O_3$ binary glass. Since Te polyhedra are present as TeO_4 and TeO_3 units, incorporation of GeO_2 can lead to a higher connectivity since Ge is known to form GeO_4 and GeO_6 units (germanium anomaly). In addition, Ge–O bonds are stronger than Te–O and Sb–O bonds, explaining Tg variations. Crystallization events were not observed in these glasses between 250 °C and 800 °C but mass losses attributed to antimony oxide or tellurium oxide evaporation were detected above this temperature, indicating a very high thermal stability against devitrification between Tg and glass evaporation around 800 °C for these samples. From this point of view, these samples can be strong candidates for manufactured devices that require high stability against

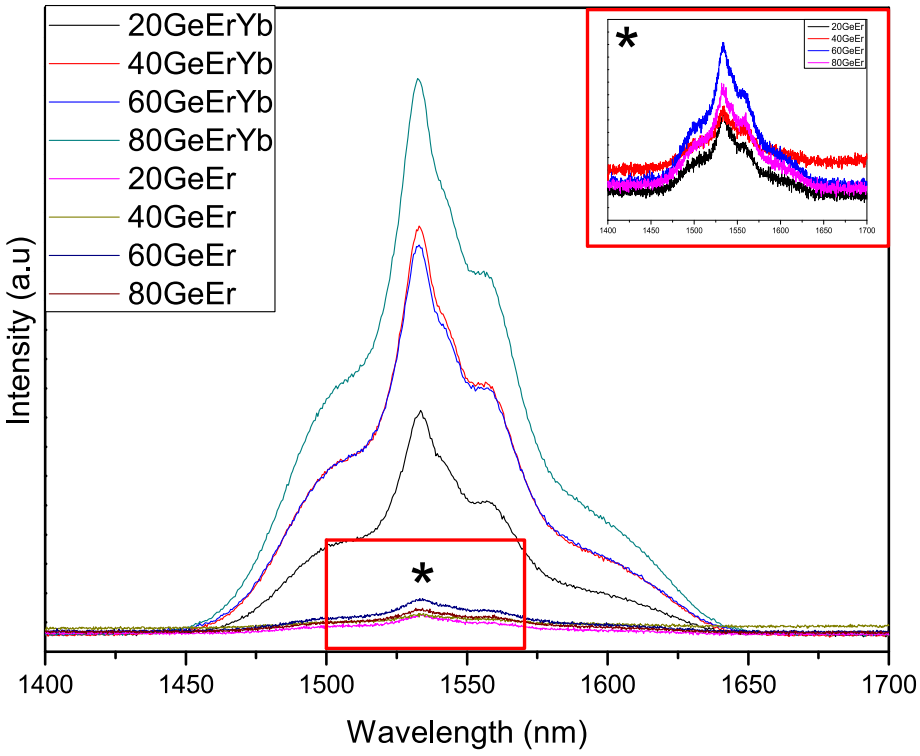

Fig. 7. Emission spectra for Er^{3+} doped and Er^{3+}/Yb^{3+} codoped glasses under 980 nm excitation.

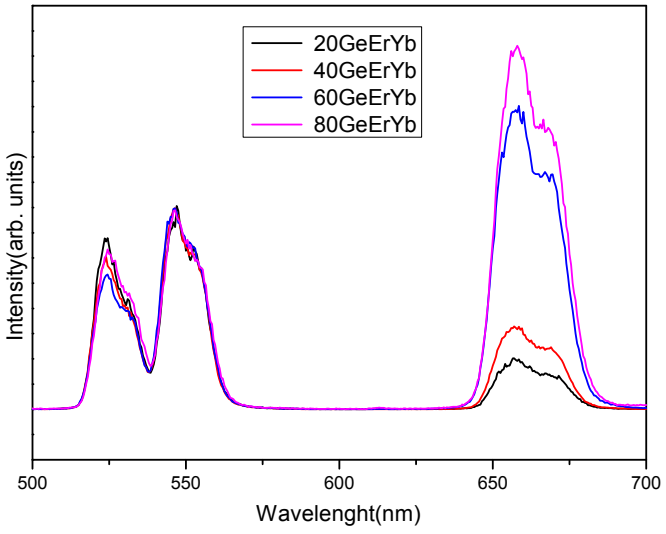

Fig. 8. Up conversion spectra for xGe samples under 980 nm laser excitation.

crystallization, with a stable visco-elastic state between 250 °C and 800 °C.

Tellurium coordination number in tellurite glasses were largely investigated by Raman and X-ray absorption spectroscopies showing that tellurium atom is surrounded by oxygen atoms in three types of sites with different geometries. For highest amounts of tellurium dioxide, the dominant tellurium sites are [TeO_4] trigonal bipyramids which are axially elongated and partly connected to each other sharing one oxygen atom. By increasing the amount of modifier oxides these units progressively convert to [TeO_3] regular trigonal pyramids through [TeO_{3+1}] entities where one axial Te—O_{ax} distance is elongated while the others shorten getting closer to the shortest equatorial Te—O_{eq} distances [39–47].

FTIR and Raman spectra presented in Figs. 3 and 4 are consistent with an overall structural change in which GeO_4 tetrahedra are progressively inserted between TeO_4, TeO_3 and SbO_3 units, increasing the network connectivity. In fact, infrared absorption band at 620 cm^{-1} related with TeO_4 units progressively vanishes whereas other bands at 850, 890 and 760 cm^{-1} due to Ge—O—Ge and Ge—O^- bonds clearly appear above 50% of GeO_2. Raman signals at 670 and 748 cm^{-1} attributed to TeO_4 and TeO_3 species respectively progressively decrease in intensity for higher GeO_2 contents whereas another Raman band at 454 cm^{-1} due to Ge—O—Ge bridging bonds shifts to lower frequencies. This behavior is in agreement with a progressive insertion of germanium oxide polyhedra inside the antimony tellurite glass network.

Absorption spectra presented in Fig. 5 revealed that these new glass compositions exhibit a wide transparency window ranging from 500 to 2200 nm, making this glasses suitable for UV, visible and NIR applications. Bandgap energies were also determined as illustrated in Fig. 6 and the values resumed in Table 1 point out that increasing GeO_2 contents lead to higher bandgap energies ranging from 3,12eV to 3,63eV. Such behavior can be related with the lower atomic number of Ge when compared to Sb and Te. Fewer atomic orbitals are available to build molecular orbitals assembled in valence and conduction bands, resulting in a higher energy gap between these bands. Refractive index as a function of composition were also measured and progressively decrease for higher GeO_2 contents as resumed in Table 1. This behavior is in agreement with a lower polarizability of the samples related with the lower atomic number of Ge substituting Sb and Te in the glass network.

Emission spectra of Er^{3+} doped and Er^{3+}/Yb^{3+} codoped glasses around 1500 nm under 980 nm excitation presented in Fig. 7 were also helpful to check the influence of Yb^{3+} on Er^{3+} emission as well as the importance of the glass matrix on emission intensities. It must be pointed out that these measurements were performed on

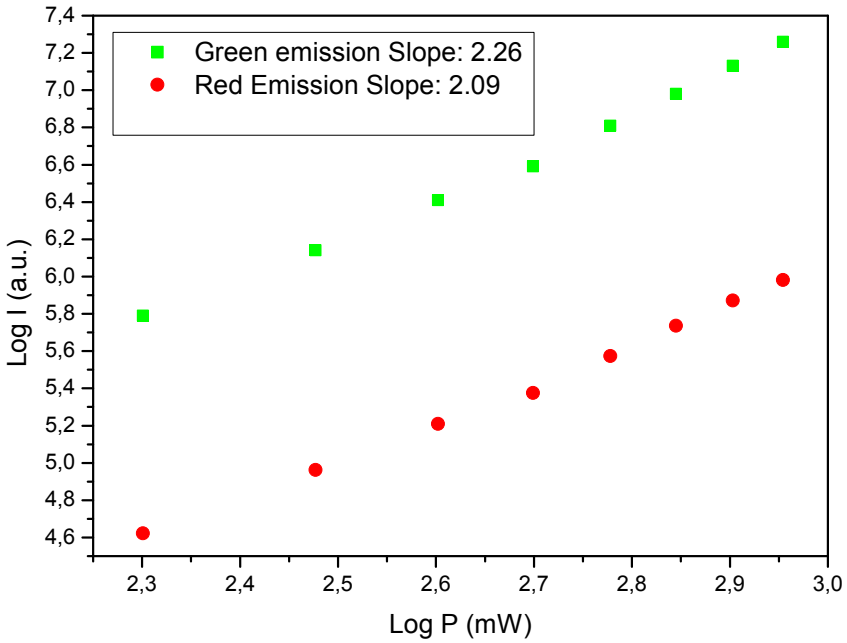

Fig. 9. Dependence of upconversion emission intensity in the red and green on excitation power under 980 nm laser excitation for 60Ge sample. (For interpretation of the references to colour in this figure legend, the reader is referred to the web version of this article.)

powder samples with the same sample quantity and shape, allowing in some extent comparison of emission band intensities. As depicted in Fig. 7, codoped samples exhibit much higher emission intensities at 1,5 μm, supporting the sensitizer behavior of Yb^{3+} for Er^{3+} emission. In fact, both rare earth ions absorb at 980 nm because of electronic transitions $^4I_{15/2} \rightarrow {}^4I_{11/2}$ in Er^{3+} and $^2F_{7/2} \rightarrow {}^2F_{5/2}$ in Yb^{3+}. However, energy level $^2F_{5/2}$ has a higher absorption cross section than $^4I_{13/2}$, absorbing the excitation photons and transferring energy to Er^{3+} to populate the $^4I_{11/2}$ energy level with a higher efficiency than direct excitation. Another important point extracted from these emission spectra is the increasing emission intensity of about two times from sample 20GeErYb to sample 80GeErYb, suggesting that richer GeO_2 environments promote more efficient radiative processes and enhancement on NIR luminescence intensity. This spectroscopic behavior is in agreement with Raman data which pointed out that GeO_2 incorporation slightly decreases the maximum phonon energy from 460 cm^{-1} to 420 cm^{-1}. Another possible explanation is the expected decrease of the glass refractive index since germanium has a lower atomic number than Te and Sb. In fact, electronic transition probabilities are strongly related with the local refractive index around the rare earth ions. Such model is also supported by the Er^{3+} decay lifetimes of energy level $^4I_{13/2}$ under excitation at 520 nm and 980 nm. Experimental luminescence decay lifetimes were determined by a first order exponential fitting of the decay curve and the results are presented in Table 2. Except for sample 60Ge, the overall tendency is an increase of the experimental lifetime for emission at 1535 nm ($^4I_{13/2} \rightarrow {}^4I_{15/2}$) from both excitations at 520 nm and 980 nm with increasing GeO_2 contents. These higher lifetimes are in agreement with lower probabilities for non-radiative relaxations promoted by lower phonon energies as well as lower expected refractive index.

Table 2
Compositions and lifetimes values for emission at 1533 nm under excitation at 520 nm and 980 nm.

Samples	Lifetime $^4I_{13/2}$ (ms) Excitation at 520 nm	Lifetime $^4I_{13/2}$ (ms) Excitation at 980 nm
20Ge	3,57	4,01
40Ge	3,83	4,24
60Ge	3,14	3,30
80Ge	4,22	4,27

Upconversion emission of these glasses in the visible under 980 nm laser excitation are presented in Fig. 8 and dependency of the emission intensity versus laser power (LogP = f(LogI)) in Fig. 9. For all emission bands at 524, 546 and 657 nm, the slope values for the linear dependency of LogP and LogI are around 2, in agreement with an upconversion mechanism in which 2 photons were absorbed for each emitted photon. Such mechanisms were already described in the literature and can be related with Energy State Absorption (ESA) or Energy Transfer Upconversion (ETU) [48–50]. ESA is related with the absorption of a first photon to populate the level $^4I_{11/2}$ and subsequent absorption of a second photon to populate the level $^4F_{7/2}$. Non radiative relaxation processes from this level populate $^2H_{11/2}$, $^4S_{3/2}$ and $^4F_{9/2}$ from whose radiative relaxations result in emissions at 524, 546 and 657 nm. In the ETU mechanism, level $^4I_{11/2}$ is also excited but some Er^{3+} ions transfer energy to other Er^{3+} ions to populate the level $^4F_{7/2}$. Subsequent relaxation processes are the same described above. Emission spectra shown in Fig. 7 also pointed out a strong dependence of the relative intensities to glass composition. As described in the experimental part, these spectra were normalized to the emission band at 546 nm for a better comparison of the relative intensities. In fact, the data clearly demonstrate that glass samples with lower GeO_2 contents exhibit a stronger green emission whereas increasing germanium oxide concentrations progressively favor a stronger red emission. Since emission at 657 nm is related with the $^4F_{9/2}$ population originated by non radiative processes from level $^4S_{3/2}$, such behavior suggests that higher GeO_2 contents form a glass matrix with a higher tendency for non radiative relaxation mechanisms. These results are of great interest since the control of composition in this system allow to control upconversion relative intensities.

5. Conclusion

Undoped, Er^{3+}-doped and Er^{3+}/Yb^{3+}-codoped glass samples were synthesized in the ternary system (80-0.8x)TeO_2-(20-0.2x) Sb_2O_3-xGeO_2 with x varying from 10 to 90. These glasses were investigated by DSC, IR, Raman, UV–Vis–NIR absorption and rare earth luminescence studies. Incorporating GeO_2 in the tellurium antimoniate glass network greatly improves the glass thermal stability and crystallization events under heating were not detected between Tg at 250 °C and 800 °C. FTIR and Raman spectroscopies depicted a structural evolution where GeO_2 six membered rings are inserted inside TeO_4 and TeO_3 units resulting in a higher connectivity of the glass network. Bandgap energy and refractive index measurements are in agreement with a lower overall polarizability of the glass network for higher GeO_2 contents. Efficiency of energy transfers from Yb^{3+} to Er^{3+} for emission around 1500 nm were demonstrated for codoped samples and it has been identified that richer GeO_2 compositions exhibit stronger emission in the infrared as well as longer luminescence decay lifetimes. Quadratic dependence of emissions at 524, 546 and 657 nm under 980 nm excitation suggest a two-photon absorption process. In addition, glasses with low GeO_2 contents present a stronger green emission whereas higher germanium oxide contents favor a stronger red emission. This study indicates that xGe glass samples may be potential materials for developing luminescent and upconversion optical devices.

Acknowledgments

The authors would like to thank brazilian funding agencies 1) FAPEMIG, 2) FINEP, 3) CNPq and 4) CAPES for financial support.

References

[1] J.E. Stanworth, Tellurite glasses, J. Soc. Glass Technol. 36 (1952) 217–241.
[2] P.L. Baynton, H. Rawson, J.E. Stanworth, Gallium oxide glasses, Nat 79 (1957) 434–435.
[3] I. Shaltout, Y. Tang, R. Braunstein, E.E. Shaisha, FTIR spectra and some optical properties of tungstate-tellurite glasses, J. Phys. Chem. Solids 9 (1996) 1223–1230.
[4] J.-C. Champarnaud-Mesjard, P. Thomas, P. Marchet, B. Frit, A. Chagraoui, A. Tairi, Glass formation study in the Bi_2O_3-TeO_2-WO_3 system, Ann. Chim. Sci. Mater 1–2 (1998) 289–292.
[5] B. Jeansannetas, S. Blanchandin, P. Thomas, P. Marchet, J.-C. Champarnaud-Mesjard, T. Merle-Mejean, B. Frit, V. Nazabal, E. Fargin, G. Le Flem, M.O. Martin, B. Bousquet, L. Canioni, S. Le Boiteux, P. Segonds, L. Sarger, Glass structure and optical nonlinearities in Thallium(I) tellurium(IV) oxide glasses, J. Solid State Chem. 2 (1999) 329–335.
[6] J.C. Sabadel, P. Armand, D. Cachau-Herreillat, P. Baldeck, O. Doclot, A. Ibanez, E. Philippot, Structural and nonlinear optical characterizations of tellurium oxide-based glasses: TeO_2-BaO-TiO_2, J. Solid State Chem. 2 (1997) 411–419.
[7] S. Blanchandin, P. Marchet, P. Thomas, J.-C. Champarnaud- Mesjard, B. Frit, A. Chagraoui, New investigations within the TeO_2-WO_3 system: phase equilibrium diagram and glass crystallization, J. Mater. Sci. 17 (1999) 4285–4292.
[8] S.H. Kim, Nonlinear optical properties of TeO_2-based glasses: Li(Na and K)$_2$O-TeO_2 binary glasses, J. Mater. Res. 3 (1999) 1074–1083.
[9] P. Charton, P. Armand, Glasses in the TeO_2-Sb_2O_4 binary system, J. Non-Cryst. Solids 2–3 (2003) 189–197.
[10] K. Shioya, T. Komatsu, H.G. Kim, R. Sato, K. Matusita, Optical properties of transparent glass-ceramics in K_2O-Nb_2O_5-TeO_2 glasses, J. Non-Cryst. Solids 1–2 (1995) 16–24.
[11] M.J. Waber, J.D. Meyers, D.H. Blackburn, Optical properties of Nd^{3+} in tellurite and phosphotellurite glasses, J. Appl. Phys. 4 (1981) 2944–2946.
[12] G. Yankov, L. Dimowa, N. Petrova, M. Tarassov, K. Dimitrov, T. Petrov, B.L. Shivachev, Synthesis, structural and non-linear optical properties of TeO_2–GeO_2–Li_2O glasses, Opt. Mater 2 (2012) 248–251.
[13] T. Miyashita, T. Manabe, Infrared optical fibers, J. Quant. Electron 10 (1982) 1432–1450.
[14] F.L. Galeener, J.C. Mikkelsen Jr., R.H. Geils, W.J. Mosby, The relative Raman cross sections of vitreous SiO_2, GeO_2, B_2O_3, and P_2O_5, Appl. Phys. Lett. 1 (1978) 34–36.
[15] A.G. Kalampounias, N.K. Nasikas, G.N. Papatheodorou, Structural investigations of the xTeO_2-(1-x)GeO_2 (x=0, 0.2, 0.4, 0.6, 0.8 and 1) tellurite glasses: a composition dependent Raman spectroscopic study, J. Phys. Chem. Solids 9 (2011) 1052–1056.
[16] C. Jiang, P. Deng, J. Zhang, F. Gan, Emission properties of ytterbium-doped GeO_2–TeO_2 glasses, Phys. Lett. A 1 (2004) 91–94.
[17] I. Endo, N. Onouchi, H. Yamaguchi, A. Shimbori, S. Matsumoto, Cathodeluminescence property of Er^{3+}/Yb^{3+}-doped amorphous GeO_2, Opt. Mater 6–7 (2006) 879–882.
[18] N. Arai, H. Tsuji, M. Hattori, M. Ohsaki, H. Kotaki, T. Ishibashi, Y. Gotoh, J. Ishikawa, Luminescence properties of Ge implanted SiO_2:Ge and GeO_2:Ge films, Appl. Surf. Sci. 4 (2009) 954–957.
[19] V.D. Cacho, L.R.P. Kassab, S.L. Oliveira, R.D. Mansano, P. Verdonck, Blue cooperative luminescence properties in Yb^{3+} doped GeO_2–PbO–Bi_2O_3 vitreous system for the production of thin films, Thin Solid Films 2 (2006) 764–767.
[20] R. Kashyap, Photosensitive optical fibers: devices and applications, Opt. Fiber Technol. 1 (1994) 17–34.
[21] D. Zelniok, C. Cramer, H. Eckert, Structure/Property correlations in ion-conducting mixed-network former glasses: solid-state NMR studies of the system Na_2O-B_2O_3-$P2O_5$, Chem. Mater 13 (2007) 3162–3170.
[22] M.R. Sahar, A. Wahab, M.A. Hussin, Structural characteristic of Na_2O P_2O_5 GeO_2 glass systems, J. Non-Cryst. Solids 11–12 (2007) 1134–1140.
[23] G.S. Henderson, R.T. Amos, The structure of alkali germanophosphate glasses by Raman spectroscopy,, J. Non-Cryst. Solids 1–3 (2003) 1–19.
[24] H.M. Wang, G.S. Henderson, O K-Edge XANES studies of alkali germanophosphate glasses, J. Non-Cryst. Solids 10–11 (2008) 863–872.
[25] S. Kumar, S. Murugavel, K.J. Rao, Absence of germanate anomaly in ternary lithium germanophosphate glasses: Modification behavior of Mixed Glass system of strong and fragile formers, J. Phys. Chem. B 25 (2001) 5862–5873.
[26] J. Ren, H. Eckert, Quantification of short and medium range order in mixed network former glasses of the System GeO_2-$NaPO_3$, J. Phys. Chem. C 23 (2012) 12747–12763.
[27] D. Ehrt, T. Kittel, M. Will, S. Nolte, A. Tunnermann, Femtosecond-laser-writing in various glasses, J. Non-Cryst. Solids 10 (2004) 332–337.
[28] T. Satyanarayana, M.G. Brik, N. Venkatramaiah, I.V. Kityk, K.J. Plucinski, V.R. Kumar, N. Veeraiah, Influence of crystallization on the luminescence characteristics of Pr^{3+} ions in PbO-Sb_2O_3-B_2O_3 glass system, J. Am. Ceram. Soc. 7 (2010) 2004–2011.
[29] K. Ouannes, M.T. Soltani, M. Poulain, G. Boulon, G. Alombert-Goget, Y. Guyot, A. Pillonnet, K. Lebbou, Spectroscopic properties of Er^{3+}-doped antimony oxide glass, J. Alloys Comp. 1 (2014) 132–135.
[30] J. Minelly, A. Ellison, Applications of antimony-silicate glasses for fiber optic amplifiers, Opt. Fiber Technol. 2 (2002) 123–138.
[31] R.A. El-Mallawany, Theoretical and experimental IR spectra of binary rare earth tellurite glasses-1, Infrared Phys. 2–4 (1989) 781–785.
[32] Y. Dimitriev, V. Dimitrov, M. Arnaudov, IR spectra and structure of tellurite glasses, J. Mar. Sci. 5 (1983) 1353–1358.
[33] P.G. Pavani, K. Sadhana, V.C. Mouli, Optical, physical and structural studies of boro-zinc tellurite glasses, Phys. B 6–7 (2011) 1242–1247.
[34] K. Błaszczak, W. Jelonek, A. Adamczyk, Infrared studies of glasses in the Li_2O–B_2O_3–$GeO_2(SiO_2)$ systems, J. Mol. Struct. 1 (1999) 163–166.
[35] P.M.V. Teja, C. Rajyasree, P.S. Rao, A.R. Babu, C. Tirupataiah, D.K. Rao, Structural and electrical properties of ZnF_2–Bi_2O_3–GeO_2 glasses doped with CoO, J. Mol. Struct. 1 (2012) 119–125.
[36] G. Monteiro, L.F. Santos, R.M. Almeida, F. D'Acapito, Local structure around Er^{3+} in GeO_2–TeO_2–Nb_2O_5–K_2O glasses and glass-ceramics, J. Non-Cryst. Solids 1 (2013) 129–136.
[37] A.J. Barbosa, et al., Er^{3+} doped phosphoniobate glasses and planar waveguides: structural and optical properties, Phys. Condens. Matter 20 (2008) 1–8.
[38] T. Som, B. Karmakar, Plasmon resonance and enchanced fluorescence application of single-step synthesized elliptical nano gold-embedded antimony glass dichroic nanocomposites, Plasmon 2 (2010) 149–159.
[39] Q.J. Rong, A. Osaka, T. Nanba, J. Takada, Y. Miura, Infrared an Raman of binary tellurite glasses containing boron and indium oxides, J. Mater. Sci. 14 (1992) 3793–3798.
[40] M. Soulis, A.P. Mirgorodsky, T. Merle- Mejean, O. Masson, P. Thomas, M. Udovic, The role of modifier's cation valence in structure properties of TeO_2-based Glasses, J. Non-Cryst. Solids 2–9 (2008) 143–149.
[41] P. Charton, P. Thomas, P. Armand, Raman and Crystallization behaviors od TeO_2-Sb_2O_4 glasses, J. Non-Cryst. Solids 1–2 (2003) 81–88.
[42] V. Nazabal, S. Todoroki, A. Nukui, T. Matsumoto, S. Suehara, T. Hondo, T. Araki, S. Inoue, C. Rivero, T. Cardinal, Oxyfluoride tellurite glasses doped by erbium: thermal analysis, structural organization and spectral properties, J. Non-Cryst. Solids 1–3 (2003) 85–102.
[43] S. Kawasaki, T. Honma, Y. Benino, T. Fujiwara, R. Sato, T. Komatsu, Writing of crystal-dots and lines by YAG laser irradiation and their morphologies in samarium tellurite glasses, J. Non-Cryst. Solids 1–3 (2003) 61–69.
[44] H. Li, Y. Su, S.K. Sundaram, Raman spectroscopic study of Nd-doped 10N_2O-90TeO_2 glasses, J. Non-Cryst. Solids 1 (2001) 402–409.
[45] T. Komatsu, H. Tawarayama, H. Mohri, K. Matusita, Properties and crystallization behaviors of TeO_2-$LiNbO_3$ glasses, J. Non-Cryst. Solids 2–3 (1991) 105–113.
[46] L. Hu, Z. Jiang, Properties and structures of TeO_2 based glasses containing ferroelectric components, Phys. Chem. Glas. 1 (1996) 19–21.
[47] M. Dimitrova-Pankova, Y. Dimitriev, M. Arnaudov, V. Dimitrov, Infrared spectral investigation of the influence of modifying oxides on the structure of

tellurite glasses, Phys. Chem. Glas. 6 (1989) 260–263.
[48] M. Pollnau, D.R. Gamelin, S.R. Lüthi, H.U. Güdel, M.P. Hehlen, Power dependence of upconversion luminescence in lanthanide and transition-metal-ion systems, Phys. Rev. B 5–1 (2000) 3337–3339.
[49] Y. Zhang, et al., Effects of GeO_2 on the thermal stability and optical properties of Er^{3+}/Yb^{3+}-codoped oxyfluoride tellurite glasses, Mater. Chem. Phys. 3 (2011) 786–790.
[50] P. Müller, M. Wermuth, H.U. Güdel, Mechanisms of near-infrared to visible upconversion in $CsCdBr_3:Ho^{3+}$, Chem. Phys. Lett. 1–3 (1998) 105–111.